CHINESE OPTICS LETTERS

Vol. 19, No. 6 | June 2021

Wideband thin-film lithium niobate modulator with low half-wave-voltage length product

Xuecheng Liu (刘学成), Bing Xiong (熊 兵)*, Changzheng Sun (孙长征), Jian Wang (王 健), Zhibiao Hao (郝智彪), Lai Wang (汪 莱), Yanjun Han (韩彦军), Hongtao Li (李洪涛), Jiadong Yu (余佳东), and Yi Luo (罗 毅)

Beijing National Research Center for Information Science and Technology (BNRist), Department of Electronic Engineering, Tsinghua University, Beijing 100084, China

*Corresponding author: bxiong@tsinghua.edu.cn

Received May 8, 2021 | Accepted May 14, 2021 | Posted Online June 25, 2021

A novel thin-film lithium niobate (TFLN) electro-optic modulator is proposed and demonstrated. $LiNbO_3$-silica hybrid waveguide is adopted to maintain low optical loss for an electrode spacing as narrow as 3 μm, resulting in a low half-wave-voltage length product of only 1.7 V·cm. Capacitively loaded traveling-wave electrodes are employed to reduce the microwave loss, while a quartz substrate is used in place of a silicon substrate to achieve velocity matching. The fabricated TFLN modulator with a 5-mm-long modulation region exhibits a half-wave voltage of 3.4 V and a merely less than 2 dB roll-off in an electro-optic response up to 67 GHz.

Keywords: lithium niobate; electro-optic modulator; wideband; half-wave voltage.
DOI: 10.3788/COL202119.060016

1. Introduction

High-speed electro-optic modulators are key devices for high-capacity fiber-optic communications[1] and microwave-photonic links[2]. Lithium niobate ($LiNbO_3$, LN) has been the preferred material for electro-optic modulators thanks to its high electro-optic coefficient ($r_{33} = 31$ pm/V), wide transmission window (340–4600 nm), and low optical loss at telecom wavelengths. However, traditional LN waveguides based on titanium in-diffusion or proton-exchange exhibit a low refractive index contrast below 0.1[3,4], which leads to large optical mode size, high bending loss, low power efficiency, and difficulty in integration. Photonic platforms based on silicon[5,6], polymers[7,8], and III-V compound semiconductors[9,10] have also been proposed, but none of them can secure wide modulation bandwidth, low drive voltage, low insertion loss, and stability simultaneously.

Recently, thin-film LN (TFLN) fabricated by crystal ion slicing and wafer bonding[11] has proved particularly attractive for realizing compact integrated devices. The high refractive index contrast of the TFLN ridge waveguide allows enhanced modulation efficiency. So far, TFLN Mach–Zehnder modulators (MZMs) with improved performances over legacy LN modulators have been demonstrated[12–16], including low half-wave voltage, large modulation bandwidth, and small footprint.

For many applications, it is desirable to further reduce the half-wave-voltage length product $V_\pi L$ and extend the modulation bandwidth of TFLN modulators. The half-wave-voltage length product for previously reported devices is mainly limited by the electrode spacing, which is mostly beyond 5 μm to avoid excessive optical absorption loss[12–16]. On the other hand, the modulation bandwidth depends critically on the microwave loss of the traveling-wave electrodes, provided that impedance matching and velocity matching are satisfied[17].

To break these performance limitations, we propose a TFLN modulator based on an LN-silica hybrid waveguide, which allows an electrode gap as narrow as 3 μm for enhanced electric field loading efficiency. Meanwhile, capacitively loaded traveling-wave electrodes (CL-TWEs) are adopted to reduce the microwave loss. Furthermore, to overcome the slow wave effect of the CL-TWEs, a quartz substrate with a low dielectric constant is employed to implement velocity matching between the microwave and the optical signals[18]. Compared with TFLN modulators on a silicon substrate[19], TFLN modulators formed on a quartz substrate are found to exhibit significantly improved high-frequency response.

2. Design and Simulation

Figure 1(a) depicts the ridge waveguide structure commonly adopted in a TFLN modulator. The refractive index variation in the X-cut LN waveguide is given by[20]

$$\Delta n_{\text{eff}} = \frac{1}{2}\Gamma\gamma_{33}n_o^3\frac{V}{g}, \tag{1}$$

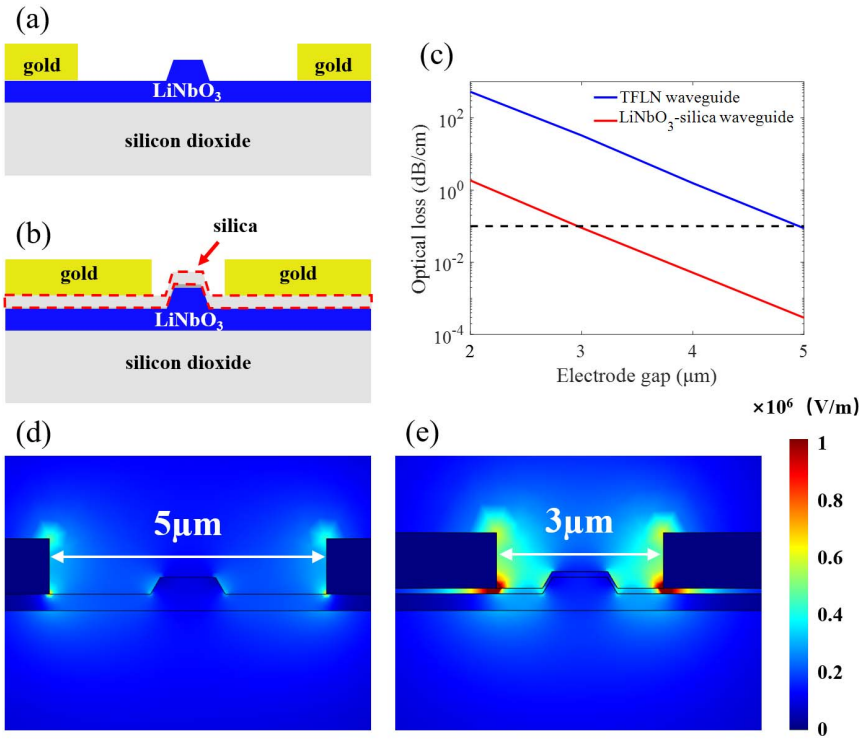

Fig. 1. (a) Conventional TFLN waveguide with wide-gap electrodes. (b) LN-silica hybrid waveguide with narrow-gap electrodes. (c) Optical absorption loss of optical waveguides with/without the silica buffer layer. RF modes in (d) TFLN waveguide with wide-gap electrodes and (e) LN-silica hybrid waveguide with narrow-gap electrodes.

where γ_{33} is the electro-optic coefficient, n_o is the optical refractive index, while V and g are the modulation voltage and the gap between the electrodes, respectively. Γ is the electro-optic overlap integral, defined as

$$\Gamma = \frac{g}{V}\frac{\iint E_e|E_o|^2 \mathrm{d}A}{\iint |E_0|^2 \mathrm{d}A}. \tag{2}$$

Here, E_e and E_o are the RF and optical field along the Z direction, respectively. Reducing the electrode spacing g helps increase Δn_{eff}, but also leads to enhanced optical loss at the metal electrodes. To avoid excessive optical loss, the electrode spacing in most TFLN modulators is beyond 5 μm, thus limiting the modulation efficiency, while silica has been used to reduce the gap between electrodes and optical waveguides[17,21]. In this work, an LN-silica hybrid waveguide is adopted[19], as shown in Fig. 1(b), which is formed by covering the partially etched LN ridge waveguide with a thin silica buffer layer. Our simulations reveal that the silica buffer layer helps suppress the leaky modes at the LN/metal interface, thus reducing the optical absorption loss at the metal electrodes dramatically (see Supplementary Material). As illustrated in Fig. 1(c), for a 1-μm-wide and 300-nm-thick partially etched ridge waveguide formed on a 600-nm-thick TFLN, the introduction of a 100-nm-thick silica buffer layer helps reduce the optical loss by more than two orders of magnitude. As a result, an optical loss of less than 0.1 dB/cm can be maintained for an electrode gap as narrow as 3 μm. As illustrated in Figs. 1(d) and 1(e), the 3-μm-spaced electrodes formed on the hybrid waveguide lead to an RF electric field enhancement of more than 40% in the LN ridge waveguide, thus reducing the half-wave voltage of the modulator effectively.

The thickness of the silica buffer layer is optimized for a trade-off between a small electrode spacing and a large electro-optic overlap factor. Assuming an upper-limit of 0.1 dB/cm for optical absorption loss, the minimum allowable electrode spacing and the corresponding electro-optic overlap factor calculated by the finite element method (FEM) are plotted in Fig. 2(a). It is evident that the minimum electrode spacing reduces rapidly as the silica buffer layer thickness increases, whereas the

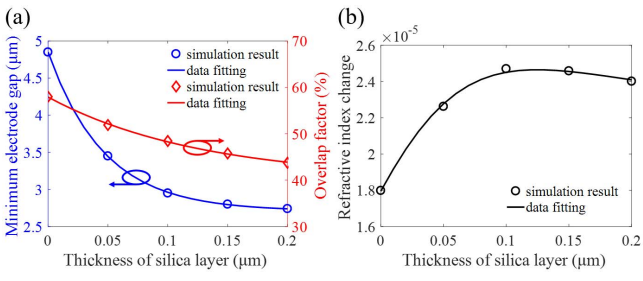

Fig. 2. (a) Minimum allowable electrode spacing and electro-optic overlap factor for different silica buffer layer thicknesses. (b) Refractive index variation of the hybrid waveguide with 1 V drive voltage. A 100-nm-thick silica layer is chosen to obtain the maximum refractive index change.

electro-optic overlap factor shows only a moderate reduction. The refractive index variation in the LN-silica hybrid waveguide under 1 V drive voltage is shown in Fig. 2(b). A 100-nm-thick silica buffer layer with an electrode spacing of 3 μm is found to provide the optimum modulation efficiency.

The key to extending the modulation bandwidth lies in reducing the microwave loss while implementing velocity and impedance matching[17]. The microwave loss of the modulator comes from the traveling-wave electrodes as well as the substrate absorption. A narrow electrode spacing facilitates electro-optic interaction, but also means a narrow signal electrode for impedance matching[22], which tends to increase the microwave transmission loss. To reduce the microwave loss while maintaining the narrow electrode gap required for low drive voltage, we adopt traveling-wave electrodes with periodically loaded T-rails, as shown in Fig. 3(a). Narrow-gap T-rails can realize high-efficiency electric field loading, while a wide signal electrode helps ensure low-loss microwave transmission. Such CL-TWEs were previously employed in III-V semiconductor electro-optic modulators[10] and have recently been proposed for TFLN modulators[18,23]. As long as the T-rails are much smaller than the microwave wavelength, they act as capacitive loadings and contribute little to the microwave transmission loss. Consequently, both wide modulation bandwidth and low half-wave voltage can be realized simultaneously, thus breaking the voltage-bandwidth limitation of TFLN modulators. As the CL-TWEs form a slow wave structure, TFLN bonded to a low dielectric constant quartz substrate is adopted instead of TFLN on silicon[12]. The quartz substrate not only helps implement velocity matching by counteracting the slow wave effect of the CL-TWEs, but also reduces the microwave loss (see Supplementary Material).

The characteristic impedance and refractive index of the traveling-wave electrodes can be expressed as

$$Z_m = \sqrt{\frac{L_0}{C_0}}, \tag{3}$$

and

$$n_m = \frac{c}{v_m} = c\sqrt{L_0 C_0}, \tag{4}$$

where C_0 and L_0 are the capacitance and inductance per unit length, respectively. Since the capacitance of the CL-TWEs mainly comes from the T-rails, whereas the inductance mainly depends on the width of the central signal electrode and the spacing between the unloaded electrodes, impedance and velocity matching can be implemented by adjusting the dimensions of the loaded/unloaded electrodes[24]. According to our FEM simulations shown in Fig. 3(b), a duty cycle of 90% is required for the T-rails spaced 3 μm apart. Figure 3(c) plots the microwave loss of the CL-TWEs as a function of the central signal electrode width. The microwave loss consists of two parts[25]: the microwave loss of the unloaded electrodes dominates for the narrow signal electrode, whereas the additional loss caused by T-rails becomes significant as the signal electrode widens, as a result of the resistance increase with a longer connection to the main electrodes. To ensure low microwave loss, the signal electrode width and unloaded electrode spacing are chosen to be 50 μm and 15 μm, respectively. In addition, the period of the T-rails is set as 50 μm, so as to ensure a large cut-off frequency in this periodic electrode structure[10].

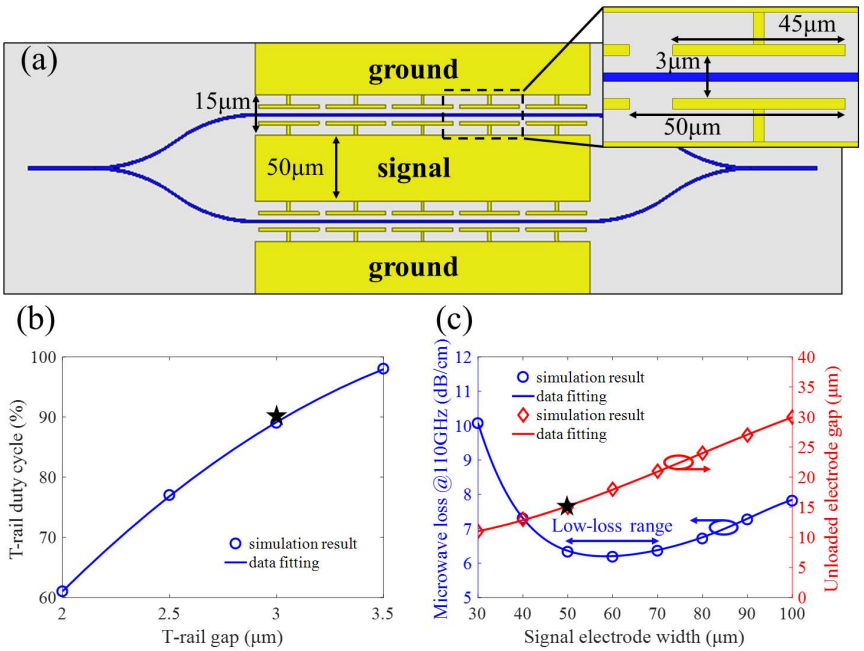

Fig. 3. (a) Top view of the CL-TWEs. (b) Duty cycle of T-rails for different T-rail gaps under capacitance matching condition. (c) Variation of microwave loss with the width of unloaded signal electrode under inductance matching condition. The star in (b) and (c) indicates the designed value.

3. Fabrication and Measurement

The modulator is fabricated with a wafer of TFLN on quartz provided by NanoLN, which includes a 2-μm-thick SiO_2 bonding layer between the 600-nm-thick *X*-cut TFLN and the 500-μm-thick quartz substrate. The optical waveguide is patterned by electron beam lithography (EBL) with hydrogensilsesquioxane (HSQ) and transferred to the TFLN by argon-based reactive ion etching (RIE). The TFLN is partially etched by 300 nm and then covered with a 100-nm-thick SiO_2 layer by plasma enhanced chemical vapor deposition (PECVD). A two-step fabrication process is employed for the CL-TWEs. First a lift-off process with polymethylmethacrylate (PMMA) exposed by EBL is employed to form T-rails with high position accuracy. Next, the main electrode patterns are defined by contact UV lithography. The main electrodes are then thickened to 1.4 μm by electroplating to reduce the microwave loss. The 3D schematic of the TFLN modulator with CL-TWEs is shown in Fig. 4(a). The scanning electron microscope (SEM) image of the T-rail electrodes is shown as the inset of Fig. 4(a). To facilitate characterization of the modulation response at high frequencies

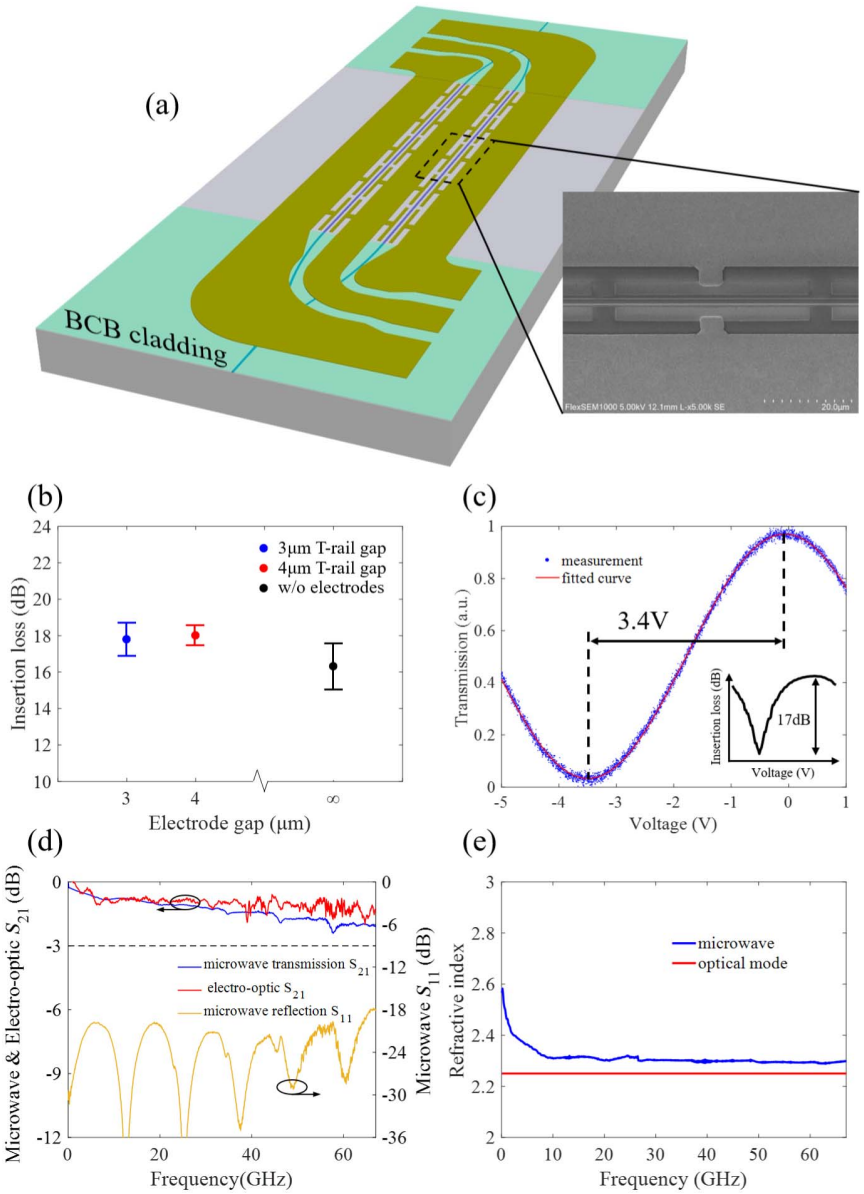

Fig. 4. (a) Demonstrated modulator 3D schematic. The unloaded electrodes have 50 μm signal electrode width, 15 μm electrode spacing, and bent tapers to match with the microwave probes. The inset shows the SEM image of the 3-μm-spaced T-rails with 50 μm period and 90% duty cycle. (b) Insertion loss of 5-mm-long modulators with different electrode gaps. (c) Normalized optical transmission as a function of modulation voltage. (d) Microwave transmission S_{21} and reflection S_{11} of the traveling-wave electrodes as well as the electro-optic response of the TFLN modulator up to 67 GHz. (e) Extracted microwave refractive index, which shows excellent matching with the group index of the optical mode ($n_g \sim 2.25$).

with microwave probes, the CL-TWEs are converted to standard coplanar waveguide (CPW) electrodes outside the modulation region. The CPW electrodes with 90° bend are formed on a 1-μm-thick benzocyclobutene (BCB) cladding layer to reduce the optical absorption (see Supplementary Material).

The performance of the modulator is tested by end-butt coupling with two tapered fibers, and a polarization controller is used to ensure TE polarized incident light at 1550 nm. In Fig. 4(b), we plot the insertion loss of 5-mm-long modulators with T-rail gaps of 3 and 4 μm. Compared with the device without electrodes, it can be concluded that the excessive optical loss due to narrow electrode gaps is effectively suppressed by the silica buffer layer, which is in agreement with the estimation shown in Fig. 1(c). The total insertion loss is measured to be 17 dB for a 5-mm-long modulator, which mainly comes from the coupling loss, as the end facets of the modulator need further polishing, and the mode field mismatch between the fiber and the optical waveguide has not been optimized. The coupling efficiency can be significantly improved by employing an inverse taper[26]. For half-wave-voltage characterization, a 100 kHz triangular wave signal is applied to the modulator, and the modulated signal is captured with a photodetector connected to an oscilloscope, as shown in Fig. 4(c). The extracted half-wave voltage for the 5-mm-long modulator is 3.4 V, together with an extinction ratio beyond 17 dB (see Supplementary Material). The half-wave-voltage length product $V_\pi L$ is as low as 1.7 V·cm, which is in excellent agreement with our simulations, mainly benefitting from the narrow electrode gap of 3 μm.

A frequency response test system with a bandwidth up to 67 GHz is used to characterize the electro-optic response of the modulator. First, the microwave transmission S_{21} and reflection S_{11} of the traveling-wave electrodes are measured by an Agilent N5227A vector network analyzer (VNA) with ground–signal–ground (GSG) microwave probes, as shown in Fig. 4(d). The microwave transmission shows a roll-off less than 2 dB up to 67 GHz, while the electrical reflection remains below −18 dB over the entire testing frequency range, indicating good impedance matching. As shown in Fig. 4(e), the extracted refractive index for the microwave signal is slightly higher than the optical group index ($n_g \sim 2.25$), which may be due to the inaccurate estimation of quartz permittivity and the fabrication deviation. Improved velocity can be implemented with a smaller duty cycle for the T-rails. To further characterize the electro-optic frequency response, the modulation signal from the VNA is fed to the modulator through a microwave probe, and the modulated signal is fed back to the VNA via a high-speed photodetector (Finisar XPDV3120R), while another microwave probe is used to provide a 50 Ω impedance termination. The electro-optic response after calibration is also plotted in Fig. 4(d). Thanks to excellent impedance and velocity matching, the modulator exhibits a smooth electro-optic frequency response with a merely less than 2 dB roll-off, and only a 1.3 dB roll off is recorded at 67 GHz, which is limited by the bandwidth of the test system. By adopting a VNA with a bandwidth up to 110 GHz (Keysight N5290A), we have verified that the microwave transmission of the traveling-wave electrodes exhibits a 6 dB bandwidth over 110 GHz, as shown in Fig. 5. Based on the extracted microwave refractive index, a 3 dB modulation bandwidth over 110 GHz is predicted (see Supplementary Material).

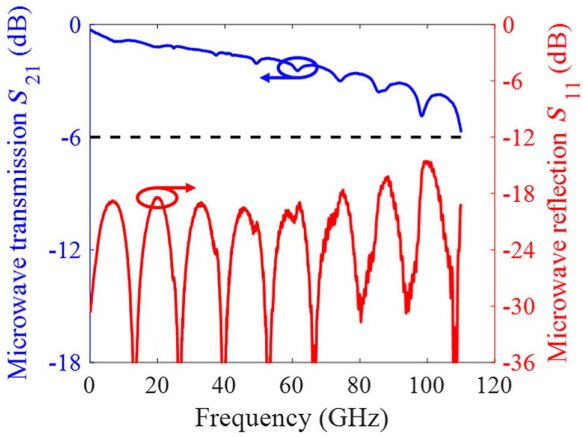

Fig. 5. Extended electrical bandwidth measurement to 110 GHz.

4. Conclusion

In this work, we have proposed a TFLN modulator structure capable of both wide modulation bandwidth and low half-wave-voltage length product. Modulators equipped with 3 μm electrode spacing CL-TWEs are fabricated on TFLN wafer bonded to a quartz substrate. A half-wave-voltage length product as low as 1.7 V·cm has been demonstrated with an LN-silica hybrid waveguide. The electro-optic response of a device with 5 mm modulation length shows a merely less than 2 dB roll-off up to 67 GHz.

Acknowledgement

This work was supported in part by the National Key R&D Program of China (No. 2018YFB2201701), National Natural Science Foundation of China (Nos. 61975093, 61927811, 61991443, 61822404, 61974080, 61904093, and 61875104), Key Lab Program of BNRist (No. BNR2019ZS01005), China Postdoctoral Science Foundation (No. 2019T120090), and Collaborative Innovation Centre of Solid-State Lighting and Energy-Saving Electronics. The authors thank Prof. Xinlun Cai of Sun Yet-sen University for help in high-frequency electro-optic response measurement.

References

1. E. L. Wooten, K. M. Kissa, A. Yi-Yan, E. J. Murphy, D. A. Lafaw, P. F. Hallemeier, D. Maack, D. V. Attanasio, D. J. Fritz, G. J. McBrien, and D. E. Bossi, "A review of lithium niobate modulators for fiber-optic communications systems," IEEE J. Sel. Top. Quantum Electron. **6**, 69 (2000).
2. J. Capmany and D. Novak, "Microwave photonics combines two worlds," Nat. Photon. **1**, 319 (2007).

3. K. Noguchi, O. Mitomi, and H. Miyazawa, "Millimeter-wave Ti:$LiNbO_3$ optical modulators," J. Lightwave Technol. **16**, 615 (1998).
4. M. Bazzan and C. Sada, "Optical waveguides in lithium niobate: recent developments and applications," Appl. Phys. Rev. **2**, 040603 (2015).
5. X. Xiao, M. Li, L. Wang, D. Chen, Q. Yang, and S. Yu, "High speed silicon photonic modulators," in *Optical Fiber Communication Conference* (OSA, 2017), paper Tu2H.1.
6. A. Khilo, C. M. Sorace, and F. X. Kärtner, "Broadband linearized silicon modulator," Opt. Express **19**, 4485 (2011).
7. J. Liu, G. Xu, F. Liu, I. Kityk, X. Liu, and Z. Zhen, "Recent advances in polymer electro-optic modulators," RSC Adv. **5**, 15784 (2015).
8. H. Miura, F. Qiu, A. M. Spring, T. Kashino, T. Kikuchi, M. Ozawa, H. Nawata, K. Odoi, and S. Yokoyama, "High thermal stability 40 GHz electro-optic polymer modulators," Opt. Express **25**, 28643 (2017).
9. R. G. Walker, "High-speed III-V semiconductor intensity modulators," IEEE J. Quantum Electron. **27**, 654 (1991).
10. Y. Ogiso, Y. Hashizume, H. Tanobe, N. Nunoya, M. Ida, Y. Miyamoto, M. Ishikawa, J. Ozaki, Y. Ueda, H. Wakita, M. Nagatani, H. Yamazaki, M. Nakamura, T. Kobayashi, and S. Kanazawa, "80-GHz bandwidth and 1.5-V V_π InP-based IQ modulator," J. Lightwave Technol. **38**, 249 (2020).
11. G. Poberaj, H. Hu, W. Sohler, and P. Günter, "Lithium niobate on insulator (LNOI) for micro-photonic devices," Laser Photon. Rev. **6**, 488 (2012).
12. C. Wang, M. Zhang, X. Chen, M. Bertrand, A. Shams-Ansari, S. Chandrasekhar, P. Winzer, and M. Lončar, "Integrated lithium niobate electro-optic modulators operating at CMOS-compatible voltages," Nature **562**, 101 (2018).
13. M. He, M. Xu, Y. Ren, J. Jian, Z. Ruan, Y. Xu, S. Gao, S. Sun, X. Wen, L. Zhou, L. Liu, C. Guo, H. Chen, S. Yu, L. Liu, and X. Cai, "High-performance hybrid silicon and lithium niobate Mach–Zehnder modulators for 100 $Gbit{\cdot}s^{-1}$ and beyond," Nat. Photon. **13**, 359 (2019).
14. X. Wang, P. O. Weigel, J. Zhao, M. Ruesing, and S. Mookherjea, "Achieving beyond-100-GHz large-signal modulation bandwidth in hybrid silicon photonics Mach Zehnder modulators using thin film lithium niobate," APL Photon. **4**, 096101 (2019).
15. A. N. R. Ahmed, S. Nelan, S. Shi, P. Yao, A. Mercante, and D. W. Prather, "Subvolt electro-optical modulator on thin-film lithium niobate and silicon nitride hybrid platform," Opt. Lett. **45**, 1112 (2020).
16. S. Sun, M. He, M. Xu, S. Gao, Z. Chen, X. Zhang, Z. Ruan, X. Wu, L. Zhou, L. Liu, C. Lu, C. Guo, L. Liu, S. Yu, and X. Cai, "Bias-drift-free Mach–Zehnder modulators based on a heterogeneous silicon and lithium niobate platform," Photon. Res. **8**, 1958 (2020).
17. A. Honardoost, F. A. Juneghani, R. Safian, and S. Fathpour, "Towards sub-terahertz bandwidth ultracompact lithium niobate electrooptic modulators," Opt. Express **27**, 6495 (2019).
18. X. Liu, B. Xiong, C. Sun, Z. Hao, L. Wang, J. Wang, Y. Han, H. Li, J. Yu, and Y. Luo, "Low half-wave-voltage thin film $LiNbO_3$ electro-optic modulator based on a compact electrode structure," in *Asia Communications and Photonics Conference (ACP/IPOC 2020)* (OSA, 2020), paper M4A.144.
19. X. Liu, B. Xiong, C. Sun, Z. Hao, L. Wang, J. Wang, Y. Han, H. Li, and Y. Luo, "Thin film $LiNbO_3$ modulator based on $LiNbO_3$-silica hybrid waveguide with narrow electrode gap," in *2020 International Topical Meeting on Microwave Photonics (MWP)* (IEEE, 2020), p. 166.
20. Y.-K. Wu and W.-S. Wang, "Design and fabrication of sidewalls-extended electrode configuration for ridged lithium niobate electrooptical modulator," J. Lightwave Technol. **26**, 286 (2008).
21. M. Jin, J. Chen, Y. Sua, P. Kumar, and Y. Huang, "Efficient electro-optical modulation on thin-film lithium niobate," Opt. Lett. **46**, 1884 (2021).
22. X. Zhang and T. Miyoshi, "Optimum design of coplanar waveguide for $LiNbO_3$ optical modulator," IEEE Trans. Microwave Theory Tech. **43**, 523 (1995).
23. P. Kharel, C. Reimer, K. Luke, L. He, and M. Zhang, "Breaking voltage–bandwidth limits in integrated lithium niobate modulators using micro-structured electrodes," Optica **8**, 357 (2021).
24. X. Liu, B. Xiong, C. Sun, Z. Hao, L. Wang, J. Wang, Y. Han, H. Li, J. Yu, and Y. Luo, "Thin film lithium niobate electro-optic modulator based on a slow wave structure," in *14th Pacific Rim Conference on Lasers and Electro-Optics (CLEO PR 2020)* (OSA, 2020), paper C4C_3.
25. J. Shin, S. R. Sakamoto, and N. Dagli, "Conductor loss of capacitively loaded slow wave electrodes for high-speed photonic devices," J. Lightwave Technol. **29**, 48 (2011).
26. L. He, M. Zhang, A. Shams-Ansari, R. Zhu, C. Wang, and L. Marko, "Low-loss fiber-to-chip interface for lithium niobate photonic integrated circuits," Opt. Lett. **44**, 2314 (2019).